NACA RM L51L03

NACA

RESEARCH MEMORANDUM

PRESSURE DISTRIBUTIONS AT MACH NUMBERS FROM 0.6 TO 1.9 MEASURED IN FREE FLIGHT ON A PARABOLIC BODY OF REVOLUTION WITH SHARPLY CONVERGENT AFTERBODY

By William E. Stoney, Jr.

Langley Aeronautical Laboratory
Langley Field, Va.

NATIONAL ADVISORY COMMITTEE
FOR AERONAUTICS

WASHINGTON

April 1, 1952
Declassified June 10, 1955

NATIONAL ADVISORY COMMITTEE FOR AERONAUTICS

RESEARCH MEMORANDUM

PRESSURE DISTRIBUTIONS AT MACH NUMBERS FROM 0.6 TO 1.9 MEASURED IN FREE FLIGHT ON A PARABOLIC BODY OF REVOLUTION WITH SHARPLY CONVERGENT AFTERBODY

By William E. Stoney, Jr.

SUMMARY

Pressure distributions were measured in a flight test of a fin-stabilized parabolic body of revolution having a sharply convergent afterbody. The fineness ratio of the body was 8.91, the maximum diameter was located at the 80-percent station, and the base area was 19.1 percent of the body frontal area. Pressure distributions were obtained continuously for Mach numbers from 0.6 to 1.9.

Pressures were measured at eight longitudinal stations over the body with and without a simulated wind-tunnel sting extending from the base of the model. The results were compared with theoretical pressures as determined by linear and exact methods. Total drag was obtained and compared with an estimated summation of the component drags. A physical picture of the flow phenomena during the passage of the model through subsonic, transonic, and supersonic Mach numbers, as deduced from the pressure measurements, is presented.

Within the limits of the test the following observations were noted: The occurrence of a shock on the afterbody, together with possible fin interference, caused rather large differences over the boattail between the experimental pressure coefficients and those calculated by both the method of characteristics and linearized theory. The total pressure drag calculated by the method of characteristics, however, agreed well with that obtained experimentally. Linearized theory gave poor agreement with the experimental pressure drag at a Mach number of 1.4. The effect of the sting was not significant except on the base of the body. The pressure midway between the fins was only slightly greater than the pressures adjacent to the fins.

INTRODUCTION

As the operating speeds of aircraft become higher, the size of the wings relative to the body become smaller, and thus the drag of the body becomes a major part of the total drag. At supersonic speeds, the pressure drag may be an appreciable part of the body drag and theoretical estimates of this drag are of great practical interest.

In flight tests conducted by the National Advisory Committee for Aeronautics on bodies of revolution differing in fineness ratio and position of maximum diameter, it was noted that linearized theory was significantly in error for bodies with sharply converging afterbodies. A preliminary test on a body identical to that of the present investigation (reference 1) indicated that the discrepancy was due mainly to the lack of agreement between the calculated and experimental pressures on the boattail. The present test was initiated to investigate this indication more fully and also to attempt to gain a general understanding of the phenomena involved in the passage of a body of revolution through the transonic flight range. As a supplement to similar wind-tunnel investigations, pressure distributions were obtained during flight with and without a simulated wind-tunnel sting attached to the base of the body.

The test was performed on a rocket-propelled body at the Pilotless Aircraft Research Station at Wallops Island, Virginia. Pressures were measured along the longitudinal axis of the body on the base and circumferentially at one station between the stabilizing fins. Total pressure and static pressure were measured on a pitot-static tube which extended 2 body diameters from the nose of the model.

The Mach number range of 0.6 to 1.9 corresponds to a Reynolds number range of 15×10^6 to 70×10^6 based on body length.

SYMBOLS

C_P pressure coefficient $\left(\frac{p - p_o}{q_o}\right)$

C_D drag coefficients based on body fontal area of 0.307 square foot

p measured pressure

p_o free-stream static pressure

q_o free-stream dynamic pressure $(0.7M^2p_o)$

M Mach number

R Reynolds number based on body length of 5.56 feet

R_m maximum radius of body, 0.312 foot

L total body length, 5.56 feet

r body radius at station x

x distance along body measured from nose

$B_M = \sqrt{M^2 - 1}$

MODEL AND TEST

The general arrangement and principal dimensions of the test configuration are shown in figure 1 and photographs of the model appear as figure 2. The profile of the body described parabolic arcs, the equations of which are as follows:

For $0 \leqq \frac{x}{L} \leqq 0.8$

$$\frac{r}{R_m} = 1 - 1.561\left(0.8 - \frac{x}{L}\right)^2$$

For $0.8 \leqq \frac{x}{L} \leqq 1.0$

$$\frac{r}{R_m} = 1 - 14.063\left(\frac{x}{L} - 0.8\right)^2$$

where R_m is the maximum radius and L is the total length.

The model had a fineness ratio of 8.91 with the maximum diameter located at the 80-percent station and had a frontal area (πR_m^2) of 0.307 square foot and a base area of 0.0586 square foot. The body was constructed of wood and finished with clear lacquer to form a smooth and fair surface. The three duralumin stabilizing fins had a total exposed area of 1.69 square feet. The fins had hexagonal sections of 0.0278 thickness ratio in the free-stream direction.

A fin-stabilized 6-inch ABL rocket was used for propulsion and was attached to the model by the sting shown in figure 1. With the exception of the 0.25-inch collar which fitted up against the base, the sting closely simulated stings used in the wind-tunnel tests of reference 2. The test sting had an L/D of 7.9 and a ratio of sting diameter to base diameter of 0.61.

The model was launched at an angle of 70° to the horizontal. Test data were obtained and reduced by the methods described in reference 3. Drag coefficients have been based on body frontal area (0.307 sq ft).

The pressures were measured at eleven 0.0625-inch-diameter orifices located as shown in figure 1. The static pressure was measured from the manifold of four 0.04-inch-diameter holes equally spaced about the pitot-static tube and located 8 tube diameters from the fore end of the sting. The total pressure orifice was 0.060 inch in diameter and was located in the hemispherical nose of the boom. The total pressure and static pressures were measured with absolute cells while the remaining pressures were measured by differential cells connected between the orifice and the static pressure from the pitot-static boom.

The model was equipped with a six-channel telemeter, four channels of which were electrically switched to record three quantities each. Fourteen quantities were recorded in all; static pressure and longitudinal acceleration were transmitted continuously and the remaining pressures were each transmitted for one third of the total time.

Pressures were measured during three different flight conditions. During powered flight, the model was attached to the booster by the simulated wind-tunnel sting shown in figure 1 and was accelerated to $M = 1.91$. This flight phase is identified in the present paper by the label "sting-on-flight." After separation of the model and booster the model decelerated from $M = 1.91$ to approximately $M = 0.2$ at which point it was at the zenith of its trajectory. During the final portion of the flight the model slowly accelerated to $M = 0.8$. These latter flight stages are referred to in the paper as "sting-off-flight" and "sting-off-accelerating flight," respectively.

Figure 3 is a plot of Reynolds number based on body length against Mach number for the three flight conditions.

DISCUSSION OF ACCURACY

The following table presents the range of errors which may be present in the pressure coefficients at the various Mach numbers and stations. The length, diameter, and arrangements of the connections

in the pressure recording system were chosen so that the lag between orifice and instrument was entirely negligible. Values for the probable errors in C_D and M are also shown.

M	ΔM	ΔC_D	ΔC_P (Possible systematic error for all stations)	Probable telemeter and data reduction error in pressure coefficients $\pm\Delta C_P$ at x/L of								
				0.175	0.450	0.625	0.800	0.850	0.910	0.950	0.975	Base
0.6	±0.005	±0.015	0.025	0.013	0.013	0.013	0.013	0.018	0.026	0.026	0.026	0.013
1.2	±.005	±.010	.025	.002	.002	.002	.002	.003	.004	.004	.004	.002
1.8	±.005	±.005	.015	.001	.001	.001	.001	.001	.002	.002	.002	.001

The possible systematic error is due to uncertainty of the boom static pressure, the record of which was somewhat different from the radiosonde measurements. The values of q_o in the pressure coefficients were computed from the radiosonde measurements since experience has indicated this method to be extremely accurate. As noted in the previous section, the body pressures were measured by differential cells attached to the static pressure from the pitot-static boom, and these measurements of ΔP were used in the pressure coefficients, as presented, since the coefficients at the 91-percent station, thus obtained, agree exactly with those obtained with an absolute cell at the same station on the identical model of reference 1. This is equivalent to the assumption that the static pressure in the boom was true static pressure but that the gage was in error, a reasonable assumption in view of successful experience with pitot-static booms of similar construction. However, the possibility exists that the pressure in the boom was as indicated by the telemeter record, in which case each value of ΔP would require correction and the systematic error in the presented data would be as shown in the table (these positive values to be added to the present data). It should be noted that the systematic errors listed in the table in no way affect the distribution of the pressure coefficients and only slightly affect their variation with Mach number.

The probable errors for C_D shown in the table refer to the drag curve obtained for the identical configuration (less pitot-static tube) in three previous tests (reference 1). This curve is used since the drag indicated by the longitudinal accelerometer in the test model was about 20 percent higher than that of the three previous models, and it is felt that the average curve for three previous models represents the drag of the configuration in the smooth condition. This conclusion is supported by the result that the average supersonic friction drag obtained by subtracting the component drags from the average total drag (reference 1) is approximately that estimated by the method of reference 4 for turbulent boundary layer. The accelerometer may have measured the drag of the configuration with a roughened surface since there is the possibility that the model was subjected to stagnation temperatures high enough to cause the clear lacquer finish to deteriorate. Since the finish could not possibly have been damaged before the model reached nearly its maximum Mach number of 1.9 and since the pressures measured before and after the peak velocity agreed remarkably well, both in level and in variation with Mach number, it is apparent that, even though the finish may have been roughened by blistering, the pressures were essentially unaffected.

RESULTS AND DISCUSSION

Basic Data and Effect of Sting

Figure 4 presents the pressure coefficients plotted against Mach number for the eight stations and the base measured on the test body and for the two stations measured on the identical configuration of reference 1. The data are presented for the three flight conditions described in the section "Models and Tests."

A comparison of the data obtained before and after separation of the model and booster shows that with the exception of the pressures at the base and at the 85- and 97.5-percent stations, the sting had little effect on the measured pressures at supersonic Mach numbers.

At subsonic velocities, the sting, as might be expected, raised the pressure at the most rearward orifices $\left(\frac{x}{L} = 0.91,\ 0.95,\ 0.975\right)$ while, with the exception of the 85-percent station where the sting-on pressure was slightly lower, it had little or no effect on those forward. At supersonic Mach numbers the effect of the sting was apparently very small at all body stations. This bears out the results of reference 2. Over the Mach number range during which the pressures changed rapidly from subsonic to supersonic values, the difference between the sting-on and sting-off data was quite large at the 97.5-percent station.

This orifice was located where the flow phenomena involved the formation (in accelerating flight) and the dissolution (in decelerating flight) of shock waves. Thus, it is possible that the pressure differences noted were the result of a difference between these two phenomena. Part of the difference may also be due to the fact that the fairing of the "sting-on" curve with respect to Mach number variation is less accurate than that of the "sting-off" curve due to the large difference between the two flight segments in the number of readings per Mach number.

The reason for the fairly large difference between the sting-on and sting-off pressures at the 85-percent station is not understood.

The sting raised the pressures on the base over the entire Mach number range. It would appear from these results that the base pressure is critically dependent on the absence or presence of a sting (of the relative size tested) even at supersonic Mach numbers.

Variation of Pressure Coefficient with Mach Number

Experimental variations.- Figure 5 presents the pressure coefficients for sting-off flight against Mach number. The critical pressure coefficient (the pressure coefficient at which the local Mach number is equal to 1) is also shown.

It is apparent that the appearance of a local Mach number of 1 at each orifice (shown by C_p critical) had no effect on the pressures there, the transition from the subsonic to the supersonic type of pressure-coefficient variation occurring at some orifices before and at other orifices after a local Mach number of 1 was reached. The nature of the transition phenomena is not clearly understood; however, a comparison of the test pressure coefficients with those of references 5 and 6 points to several qualitative trends which appear to be of general applicability. The following remarks, while illustrated by the pressures on the test model, apply also to the data of references 5 and 6.

The manner in which the transition occurred depended on whether the location of the orifice was behind or ahead of the body position at which a local Mach number of 1 was first attained. On the test model, a local Mach number of 1 was first reached at or near the 85-percent station. The transition of the pressures ahead of this critical station was generally accompanied by a rise in the level of the pressure coefficients while the transition at the orifices to the rear of the critical station was characterized by a decrease in the pressures. The transition at these rear orifices was further differentiated from that at the forward orifices by its greater magnitude

and sharpness and by the presence of a small positive peak which occurred before the sudden decrease. As the transition of all the most rearward orifices $\left(\frac{x}{L} = 0.95, 0.975, 0.996\right)$ began at approximately the same free-stream Mach number (and totally different local Mach numbers), it would appear that the transition at these orifices was caused by the transition of the pressure at some point closer to the critical position.

Comparison of experimental and theoretical variations.- The variations of the sting-off flight pressure coefficients with Mach number are compared with theoretical variations in figure 6.

The supersonic theoretical variations were calculated by modifying the experimental pressure coefficient at $M = 1.4$ as follows:

From Laitone (reference 7)

$$C_{P_M} = C_{P_{1.4}} \frac{\log\left(B_M \frac{r}{x}\right)}{\log\left(B_{1.4} \frac{r}{x}\right)} \tag{1}$$

and empirically (based on present data)

$$C_{P_M} = C_{P_{1.4}}\left(\frac{1.4}{M}\right)^{3/2} \tag{2}$$

To the approximations of reference 7 the pressure coefficient is constant above $M = 1.4$. For the present comparison, however, the variation of equation (1) for Mach numbers below 1.4 was extended to the higher Mach numbers since it was apparent that better agreement was obtained in this manner. Where the absolute value of the pressure coefficient is fairly small both methods agree reasonably well with the experimental pressure coefficients. Where the pressure coefficients are large, as at the orifices on the boattail, the empirical curve of equation (2) gives the better approximation. At the 97.5 station the pressure coefficient variation between $M = 1$ and 1.4 was caused by the passage of a shock band over the orifice (this will be discussed in a following section) and thus neither theoretical method can be expected to agree with the measurements in this range. A comparison of the two methods with the data of reference 5 leads to the same conclusion with regard to the applicability of the methods. Thus, while equation (2) is entirely empirical, it appears from the limited comparison made that it provides a good approximation in the range shown ($M = 1.1$ to 1.9).

The subsonic theoretical variations were calculated by the method of Lees (reference 8) by using the incompressible solution of reference 9 as a base. The level of the theoretical values is mainly dependent on the theoretical values of the incompressible pressure coefficients used (reference 9). As can be seen from the figure, the variations of the theoretical and experimental pressure coefficients with Mach number are similar and it thus appears likely that better agreement than shown in figure 6 would be obtained if low Mach number experimental pressure coefficients were used in Lees's variation equations. Though Lees's method was derived only for the pressure at the maximum diameter of ellipsoids, wind-tunnel tests (reference 10) have shown it to predict closely the variations of the pressures over bodies of varying shapes. The present results further substantiate the general applicability of Lees's method.

Pressure Distributions

Experimental longitudinal pressure distributions.- The plots in figure 7 present the pressure distributions along the body at varying free-stream Mach numbers. The results are presented in three Mach number groups: (a) subsonic, (b) supersonic, and (c) transonic Mach numbers.

The symbols represent the eight pressures measured in the present test and the pressure measured at the 99.6-percent station on the identical body of reference 1. Base-pressure coefficients are shown by solid symbols. Theoretical points calculated for the nose without the pitot-static tube by the methods of references 8, 9, and 11 are also included.

From a comparison of the figures it can be seen that, as the Mach number increased from subsonic to transonic values, the low-peak suctions occurring a little behind the maximum diameter increased in value. Between Mach numbers of 0.925 and 0.975 the increase in peak suctions was accompanied by a rearward movement of the peak value. This corresponds to the beginning of the drag rise. Above a Mach number of 0.975 the peak suction decreased while continuing to move rearward.

At subsonic and supersonic speeds the pressures over the nose varied little with Mach number. The rapid increase of pressure at the 80-percent station during the transonic range indicates the decreasing influence of the afterbody shape on the pressures forward.

The relationship between the base-pressure and the side-pressure coefficients at the 99.6-percent station indicates that the variation of the base-pressure coefficients with Mach number are in general

dependent on the variation of the pressure coefficients at the 99.6-percent station. This result was also noted in reference 12.

Experimental circumferential pressure distributions.- The circumferential distribution of the pressures between the fins is shown in figure 8. As the figure shows, the pressures were slightly higher midway between the fins than at their base. Similarly small circumferential variations were obtained in the tests of reference 13. The circumferential variation in pressure noted was not great enough to affect materially the calculation of pressure drag obtained by using only the pressures on the center line between the fins.

Comparison of experimental and theoretical longitudinal pressure distributions.- Figure 9(a) presents a comparison of the experimental pressure distribution at $M = 1.4$ with theoretical distributions calculated by (1) the method of characteristics (reference 14) coupled with the conical values for the forepart of the nose (reference 11), (2) the linearized method of Von Kármán and Moore (reference 15), and (3) for the nose section only, the slender-body theory of Lighthill (reference 16).

The difference between the theoretical and experimental pressures over the nose is somewhat larger than that obtained over other forebodies of similar fineness ratio ($n \approx 7$, references 17 and 18). This consideration, together with the fact that the experimental distribution gives negative pressure drag over the nose at supersonic speeds indicates that the level of the forebody pressures, as measured, may be too low. Reference 19 showed that the method of characteristics gives accuracies of 2 percent in velocity even with relatively coarse meshes and that as the lattice size is decreased, the solution approaches the correct solution from one direction only. Thus, it appears that the bumps in the present calculations are the result of changing lattice size (indicated by the spacing of the symbols) and that the increasing difference between the experimental and theoretical values over the nose may be due, in part, to increasing the lattice size over the rear part of the forebody.

Over the nose all three theoretical calculations were in good agreement. Lighthill's method gives a closed solution for bodies with analytic meridians and thus is by far the easiest of the three to apply. It appears for bodies near the fineness ratio of the test forebody ($n \approx 7$) that this method is the most practical. A similar conclusion was reached in reference 18.

Over the boattail the differences between the experiment and the theoretical calculations were the result of complex flow phenomena which are beyond the scope of the theories used. In addition, the linear assumptions of the Von Kármán-Moore method cannot be expected

to hold over the extreme curvature of the test boattail. The difference between the experimental and method-of-characteristics pressure coefficients over the rear section of the afterbody may have been due to the presence of a shock wave on this area (this will be discussed in the following section) which caused the high recompression not predicted by the theory. In the region ahead of the possible shock $\left(0.8 < \frac{x}{L} < 0.95\right)$ the difference may have been due to fin interference. Wind-tunnel tests of a parabolic body with and without four sweptback fins (reference 13) indicate (with consideration that the fins of the present paper differ in number, thickness, and profile from those of the reference paper) that the influence of the fins on the boattail pressures can be of the magnitude of the differences previously noted.

Figure 9(b) compares the experimental pressure distribution at $M = 1.8$ with the distribution calculated by the method of characteristics. The agreement between the theory and the experimental values on the nose was appreciably better at this Mach number. The differences between the theory and the experiment over the afterbody are probably due mainly to fin interference, since the shock wave which caused the high pressure recovery at $M = 1.4$ has probably moved off the body by $M = 1.8$. At both $M = 1.4$ and 1.8 the method of characteristics closely predicted the position of the minimum pressure.

Figure 9(c) compares the experimental pressure distribution at $M = 0.7$ with a theoretical distribution for the same Mach number. The theoretical distribution consists of the incompressible solution of reference 9 corrected for the effects of compressibility by the method of reference 8. The good agreement of the experimental results with the theory over the afterbody indicates that there was no appreciable separation.

Velocity Distribution and Discussion of Flow Phenomena

The flow description presented in the following paragraphs is assumed to apply to the body without fins. The effect of the fins on the pressure distributions from which this description is deduced is not known. However, since the fins were thin (2.78 percent) it is assumed that their effect was small and, thus, that the general flow description applies to bodies without fins. This conclusion is further justified by the similar flow phenomena noted in reference 5 on a body with fins located on a trailing boom.

The flow picture is most graphically shown in figure 10, where the changes in the local Mach numbers with free-stream Mach numbers (M_f) are presented. The local Mach numbers were calculated from the pressure coefficients and the free-stream Mach numbers. Since the effect

of the entropy gain through the bow shock wave is reasonably small at the Mach numbers considered, this factor was neglected in the calculations.

As can be seen from the velocity distributions the flow reached a local Mach number of 1.0 at a free-stream Mach number of approximately 0.87 at the 85-percent body station. As the free-stream Mach number increased, the region of local supersonic flow on the body expanded both forward and rearward from the 85-percent station. The similarity of the velocity profiles up to $M_f = 0.92$ indicates that the flow was without disturbances until this speed. At $M_f = 0.94$ the break in the velocity profile and the high velocity gradients before the break indicate the formation of a normal shock between the 91- and 95-percent stations. It can be seen from figure 5 that the pressure coefficients at the three rearward orifices started to decrease at about this Mach number ($M_f \approx 0.95$) while the coefficients at the 91-percent station (located ahead of the possible shock wave) showed no effect of the changes occurring at the downstream orifices at $M_f = 0.95$. With increasing M_f the peak velocity moved rearward, the velocity gradient became slightly less, and the break in the velocity profile disappeared. Thus, it appears that the shock became oblique and moved rearward with increasing M_f. Because of the interaction of the shock and the boundary layer, the pressures at the body surface were felt as a finite band of compression waves. The steadily decreasing pressure rise between the 95- and 97.5-percent stations (see fig. 5) and the steadily increasing pressure rise between the 97.5- and 99.5-percent stations indicate the movement of this compression band from a position entirely between the 95- and 97.5-percent stations (at $M_f \approx 1.00$) to a position between the 97.5- and 99.6-percent stations at an M_f of about 1.4. It would seem reasonable to assume that, with further increases in free-stream Mach number, the shock and compression band moved off and downstream of the afterbody. Such a movement is indicated by the sudden decrease in pressure coefficients at the 99.6-percent station at $M = 1.43$. However, the pressure coefficients at this orifice were obtained on the model of reference 1 which contained a sustainer rocket, afterburning of which may have influenced the pressures during this Mach number range and thus may have caused the pressure coefficients at the 99.6-percent station to be unreliable above $M = 1.43$.

It can be seen from the velocity distributions that the forward spread of the supersonic flow field was not accompanied by any disturbances. This difference in the transition at the forward and tailing edges of the supersonic "bubble" may account for the differences in the character of the transitions of the pressure coefficients at the stations before and after the 85-percent station shown in figure 5.

It appears from the present analysis and from the data of references 5 and 20 that the formation of a shock at the rear edge of the supersonic bubble is a general occurrence on bodies of revolution and is similar to such formations on wings. It also appears that the location of such a shock is a function of boattail convergence (as indicated by the tests of references 12 and 20) and a function of Mach number (as indicated by the present test and reference 5).

In addition to illustrating the flow phenomena discussed previously, the velocity distributions indicate velocity profiles (and similarly pressure profiles) over the nose at supersonic speeds that, because they are partially concave, appear incompatible with theoretical calculations. This incompatability may perhaps be due to a phenomenon noted in reference 18. In this reference mention is made of a "hump" not predicted by theory which has been measured on various nose shapes (references 5, 15, 17, 21, and 22) and which appears to be characteristic of slender bodies of revolution. The few pressures measured on the nose of the present test vehicle could not be expected to show such a hump in the distribution. However, the reflex in the pressure- and velocity-distribution curves, which is characteristic of the supersonic profiles in the present test, may well have been caused by the attempt to fair a smooth line over a normally curved distribution which included the hump just mentioned.

Drag

Figure 11(a) is a plot of nose, boattail, and total pressure drag against Mach number. This figure indicates that the forebody was contributing a small amount of thrust during most of the flight range. Theoretical considerations indicate that such a condition is impossible at supersonic speeds. It is felt that the present results are due mainly to a small inaccuracy in the level of the pressure distributions coupled with errors in the integration of the nose pressures due to fairing of the pressure distributions. The accuracy of the quantities is, however, good enough to indicate the relative proportion of the nose and boattail pressure drags and to show this variation with Mach number.

Figure 11(b) presents the pressure-drag distribution at $M = 1.4$ calculated by the following formula with the use of the three pressure distributions: (a) the method of characteristics, (b) Von Kármán-Moore, and (c) experimental.

$$\frac{dC_D}{d(x/L)} = \frac{2L}{R_m^2} C_{pr} \frac{dr}{dx}$$

The figure clearly shows that the major portion of the drag was developed over the afterbody although some degree of error in the distribution is indicated by the negative nose drag. As mentioned in the section "Discussion of Accuracy" there possibly was a systematic error in the level of the pressure data such that the pressure data, as presented, may be low over the entire body. Since such a shift would not greatly affect the total pressure drag, the close agreement between the total pressure drag from experiment and from the method of characteristics may not be as fortuitous as a comparison of the drag distribution might indicate. Though the experimental pressure distribution over the tail is different from that calculated by the method of characteristics, because of the presence of a shock and of fin interference, it appears that differences of this nature may not be enough to affect seriously the calculation of the pressure drag. The possible shift in level is in a direction such that, were it applied, the experimental drags over both nose and boattail would approach that calculated by the method of characteristics, and it would cause a larger difference between the experimental boattail drag and that calculated by the linearized method. The lack of agreement between the linearized calculations and the experimental pressure over the afterbody might be expected from consideration of the large curvature of the body in this region.

Figure 11(c) presents, as a function of Mach number, the total drag broken down into its various components: base, fin, pressure, and friction drag. The breakdown is not intended to be rigorous, because of the necessary roughness with which the various components were calculated. However, the results are believed to show very well the relative variation of the components with Mach number as well as the mechanism of the drag rise.

The total drag shown is taken from the average curve for three identical configurations (less pitot-static tube) reported in reference 1. This was necessary because the drag curve for the test model was considerably higher than that obtained on the three previous models. (See section "Discussion of Accuracy.")

The base drag was calculated from the base-pressure measurements by assuming that the measured pressure was acting over the whole base. The isolated fin drag was measured in flight on a cylindrical body by the use of the technique described in reference 3. The pressure drag was obtained from integration of the pressure distributions over the body.

Figure 11(a) and (c) shows clearly that the abrupt transition to high supersonic drag is primarily due to the increased suctions over the afterbody. The manner in which the peak suction builds up and moves rearward (the rearward movement also increasing the drag component) has been discussed in the section concerning the transonic pressure distributions.

The discontinuity in the pressure drag at $M = 0.965$ caused by a fluctuation in the pressures over the boattail resembles dips noted in the total-drag variation with Mach number of winged parabolic-arc bodies (reference 23 and unpublished data). The dip does not appear in the total-drag curve presented because the velocimeter radar with which the drag was obtained is unable to record sudden variations in acceleration (see reference 3); however, the longitudinal accelerometer in the present model did indicate the presence of such a dip. Thus it would appear that the drag breaks observed on the winged reference models are also due to the fluctuations of the suction pressures over the boattail. This fluctuation in suction pressures may be due (on the test configuration) to the formation of the shock wave on the afterbody.

The friction drag, shown as the difference between the total drag and the sum of the component drags remains fairly constant throughout the Mach number range except during the drag rise, where, as mentioned before, the values of total drag are the least reliable, because of the inaccuracy of the velocimeter radar in measuring rapidly changing accelerations. While the value of the friction drag coefficient is about that predicted by the method of reference 4 ($C_f = 0.05$), it is obvious that its variation with Mach number does not correspond to the theoretical estimates. It is felt that this discrepancy is due to the inaccuracies in the component drags.

CONCLUDING REMARKS

A fin-stabilized body of revolution was flight tested to obtain the longitudinal pressure distributions at Mach numbers from 0.6 to 1.9. Pressures were obtained with and without a simulated wind-tunnel sting attached to the base of the model.

A physical picture of the flow about the test configuration has been deduced from consideration of the pressure and local velocity distributions with the assumption of negligible fin effect on the afterbody pressures. A brief summary of the flow picture follows.

As the body reached high subsonic Mach numbers, the flow attained a local Mach number of 1.0 at a point on the body a bit behind the maximum diameter. As the Mach number increased the region of local supersonic flow spreads forward and rearward over the body. While the transition between subsonic and supersonic flow occurred smoothly at the fore edge of the supersonic "bubble," the phenomenon at the rear edge was quite complex. At a free-stream Mach number of about 0.94, a normal shock formed in the region between the 91- and 95-percent stations coincident with a sudden decrease in the pressure coefficients at all orifices downstream of the 91-percent station. With further

increase in Mach number, the shock became oblique and attached to the body by a fan of compression waves. This compression band moved rearward over the boattail with increasing Mach number and at a Mach number of 1.45 was located approximately between the 97.5- and 99.6-percent stations. As the Mach number increased still further the shock may have moved downstream and off the body entirely, but this could not be absolutely determined from the present test data.

It appears from the present and similar tests that the formation of a shock on the afterbody during transonic Mach numbers is a phenomenon that is common to all boattailed shapes. The location of the shock appears from the present test to be a function of Mach number and from previous tests to be closely associated with the afterbody convergence.

A comparison of the measured pressures with those calculated by various theoretical methods permits the following observations to be made: The occurrence of a shock on the afterbody, together with possible fin interference caused rather large differences over the boattail between the experimental pressure coefficients and those calculated by both the method of characteristics and linearized theory. The total pressure drag calculated by the method of characteristics, however, agreed well with that obtained experimentally. Linearized theory gave poor agreement with the experimental pressure drag at a Mach number of 1.4.

The variation of the pressure coefficients with supersonic Mach numbers was found to be best approximated by an empirical relationship. Laitone's method was found to give large errors at orifices measuring high suctions. The variation of subsonic pressure coefficients with Mach number agreed well with the method of Lees.

Separation of the total drag into its various components showed that the major portion of the drag at supersonic speeds came from the high suctions over the boattail and that the drag rise was caused mainly by the sudden increase in the suctions over this portion of the body.

The data obtained with and without a simulated wind-tunnel sting attached to the base of the model indicate the following conclusions: At supersonic speeds the sting had no appreciable effect on the pressures over the body. The sting raised the pressures on the base at nearly all Mach numbers. This effect diminished with increasing Mach number.

The pressure midway between the fins was only slightly greater than the pressure adjacent to the fins at the 50-percent fin station.

Langley Aeronautical Laboratory
National Advisory Committee for Aeronautics
Langley Field, Va.

REFERENCES

1. Stoney, William E., Jr., and Katz, Ellis: Pressure Measurements on a Sharply Converging Fuselage Afterbody with Jet On and Off at Mach Numbers from 0.8 to 1.6. NACA RM L50F06, 1950.

2. Perkins, Edward W.: Experimental Investigation of the Effects of Support Interference on the Drag of Bodies of Revolution at a Mach Number of 1.5. NACA RM A8B05, 1948.

3. Morrow, John D., and Katz, Ellis: Flight Investigation at Mach Numbers from 0.6 to 1.7 to Determine Drag and Base Pressures on a Blunt-Trailing-Edge Airfoil and Drag of Diamond and Circular-Arc Airfoils at Zero Lift. NACA RM L50E19a, 1950.

4. Van Driest, E. R.: Turbulent Boundary Layer in Compressible Fluids. Jour. Aero. Sci., vol. 18, no. 3, March 1951, pp. 145-160.

5. Thompson, Jim Rogers: Measurements of the Drag and Pressure Distribution on a Body of Revolution throughout Transition from Subsonic to Supersonic Speeds. NACA RM L9J27, 1950.

6. Danforth, Edward C. B., and Johnston, J. Ford: Pressure Distribution over a Sharp-Nose Body of Revolution at Transonic Speeds by the NACA Wing-Flow Method. NACA RM L7K12, 1948.

7. Laitone, E. V.: The Linearized Subsonic and Supersonic Flow about Inclined Slender Bodies of Revolution. Jour. Aero. Sci., vol. 14, no. 11, Nov. 1947, pp. 631-642.

8. Lees, Lester: A Discussion of the Application of the Prandtl-Glauert Method to Subsonic Compressible Flow over a Slender Body of Revolution. NACA TN 1127, 1946.

9. Von Kármán, Theodor: Calculation of Pressure Distribution on Airship Hulls. NACA TM 574, 1930.

10. Matthews, Clarence W.: A Comparison of the Experimental Subsonic Pressure Distributions about Several Bodies of Revolution with Pressure Distributions Computed by Means of Linearized Theory. NACA TN 2519, 1951.

11. Staff of the Computing Section, Center of Analysis (Under Direction of Zdeněk Kopal): Tables of Supersonic Flow around Cones. Tech. Rep. No. 1, M.I.T., 1947.

12. Katz, Ellis R., and Stoney, William E., Jr.: Base Pressures Measured on Several Parabolic-Arc Bodies of Revolution in Free Flight at Mach Numbers from 0.8 to 1.4 and at Large Reynolds Numbers. NACA RM L51F29, 1951.

13. Hasel, Lowell E, Sinclair, Archibald R., and Hamilton, Clyde, V.: Preliminary Investigation of the Drag Characteristics of the NACA RM-10 Missile at Mach Numbers of 1.40 and 1.59 in the Langley 4- by 4-Foot Supersonic Tunnel. NACA RM L52A14, 1952.

14. Ferri, Antonio: Application of the Method of Characteristics to Supersonic Rotational Flow. NACA Rep. 841, 1946. (Formerly NACA TN 1135.)

15. Von Kármán, Theodor, and Moore, Norton B.: Resistance of Slender Bodies Moving with Supersonic Velocities with Special Reference to Projectiles. Trans. A.S.M.E., vol. 54, no. 23, Dec. 15, 1932, pp. 303-310.

16. Lighthill, M. J.: Supersonic Flow past Bodies of Revolution. R. & M. No. 2003, British A.R.C., 1945.

17. Luidens, Roger W., and Simon, Paul C.: Aerodynamic Characteristics of NACA RM-10 Missile in 8- by 6-Foot Supersonic Wind Tunnel at Mach Numbers from 1.49 to 1.98. I - Presentation and Analysis of Pressure Measurements (Stabilizing Fins Removed). NACA RM E50D10, 1950.

18. Love, Eugene S.: Aerodynamic Investigation of a Parabolic Body of Revolution at Mach Number of 1.92 and Some Effects of an Annular Jet Exhausting from the Base. NACA RM L9K09, 1950.

19. Liepmann, H. W., and Lapin, Ellis: Summary of Characteristics Methods for Steady State Supersonic Flows. Rep. No. SM-13343, Douglas Aircraft Co., Inc., March 3, 1949.

20. Chapman, Dean R., and Perkins, Edward W.: Experimental Investigation of the Effects of Viscosity on the Drag of Bodies of Revolution at a Mach Number of 1.5. NACA RM A7A31a, 1947.

21. Dorrance, W. N.: A Supersonic Body Profile Developmental Study. Report No. 2 - First Order and Linearized Theories for Supersonic Flow around Bodies of Revolution with Experiments at Mach Number 1.90. Rep. No. UMM-54, Aero. Res. Center, Univ. of Michigan, June 1, 1950.

22. Ferri, Antonio: Supersonic-Tunnel Tests of Projectiles in Germany and Italy. NACA ACR L5H08, 1945.

23. Schult, Eugene D.: Large-Scale Flight Measurements of Zero-Lift Drag at Mach Numbers from 0.8 to 1.6 of a Wing-Body Combination Having an Unswept 4.5-Percent-Thick Wing with Modified Hexagonal Sections. NACA RM L51A15, 1951.

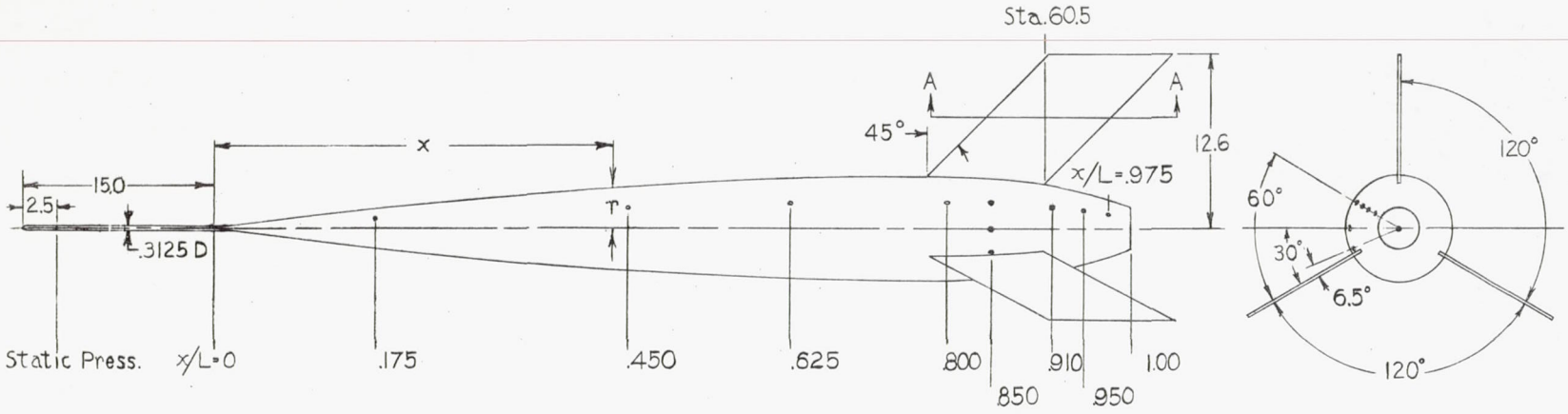

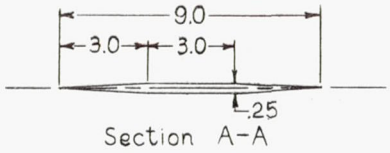

x	r	x	r
8.0	1.04	56.0	3.67
16.0	1.91	58.0	3.51
24.0	2.61	60.0	3.24
33.0	3.20	62.0	2.89
40.0	3.51	64.0	2.43
47.0	3.70	66.0	1.89
50.0	3.73	66.8	1.64
53.4	3.75		

(a) Location of pressure orifices.

Figure 1.- General arrangement of model and sting. (All dimensions are in inches.)

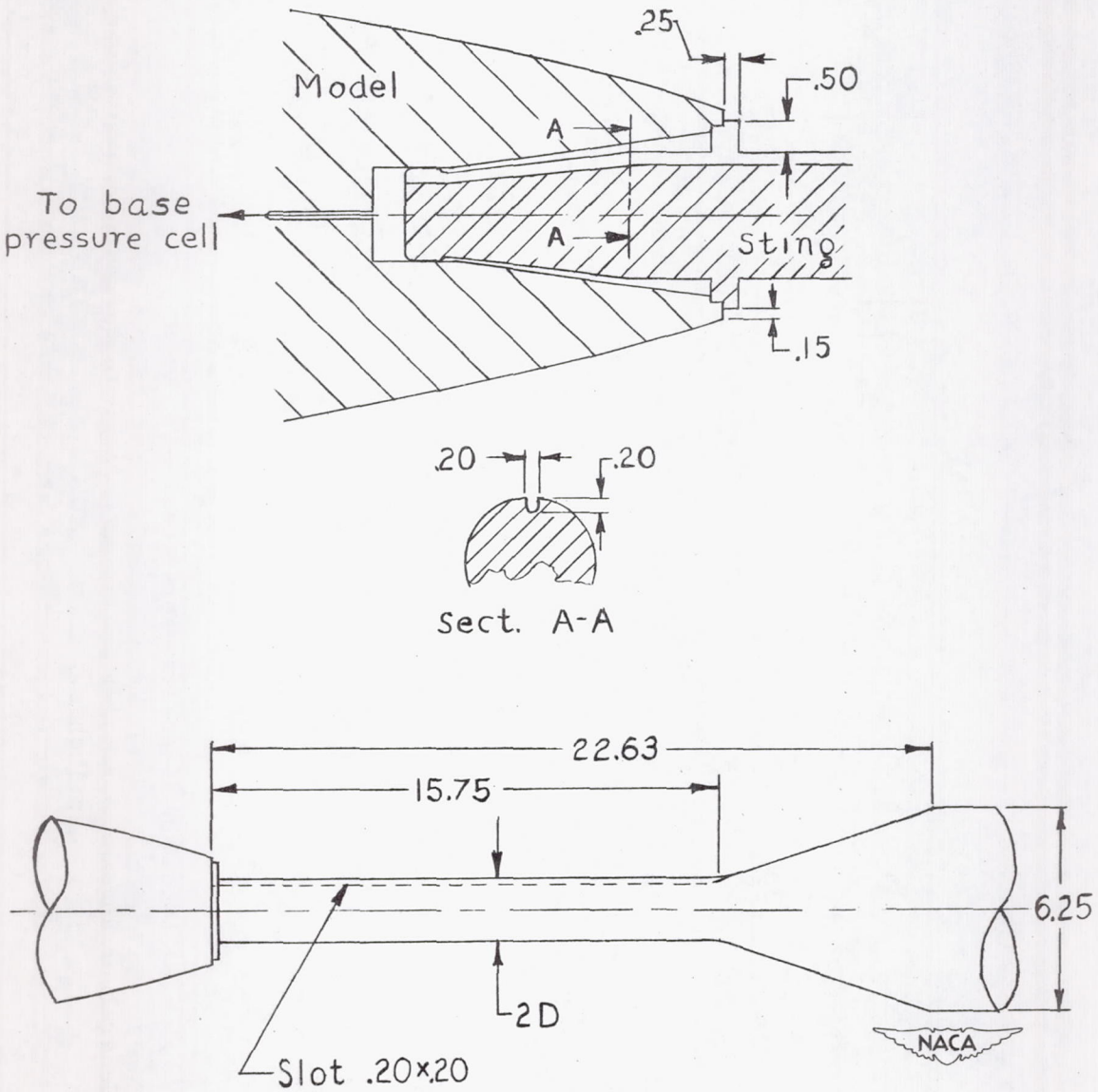

(b) Sting between model and booster.

Figure 1.- Concluded.

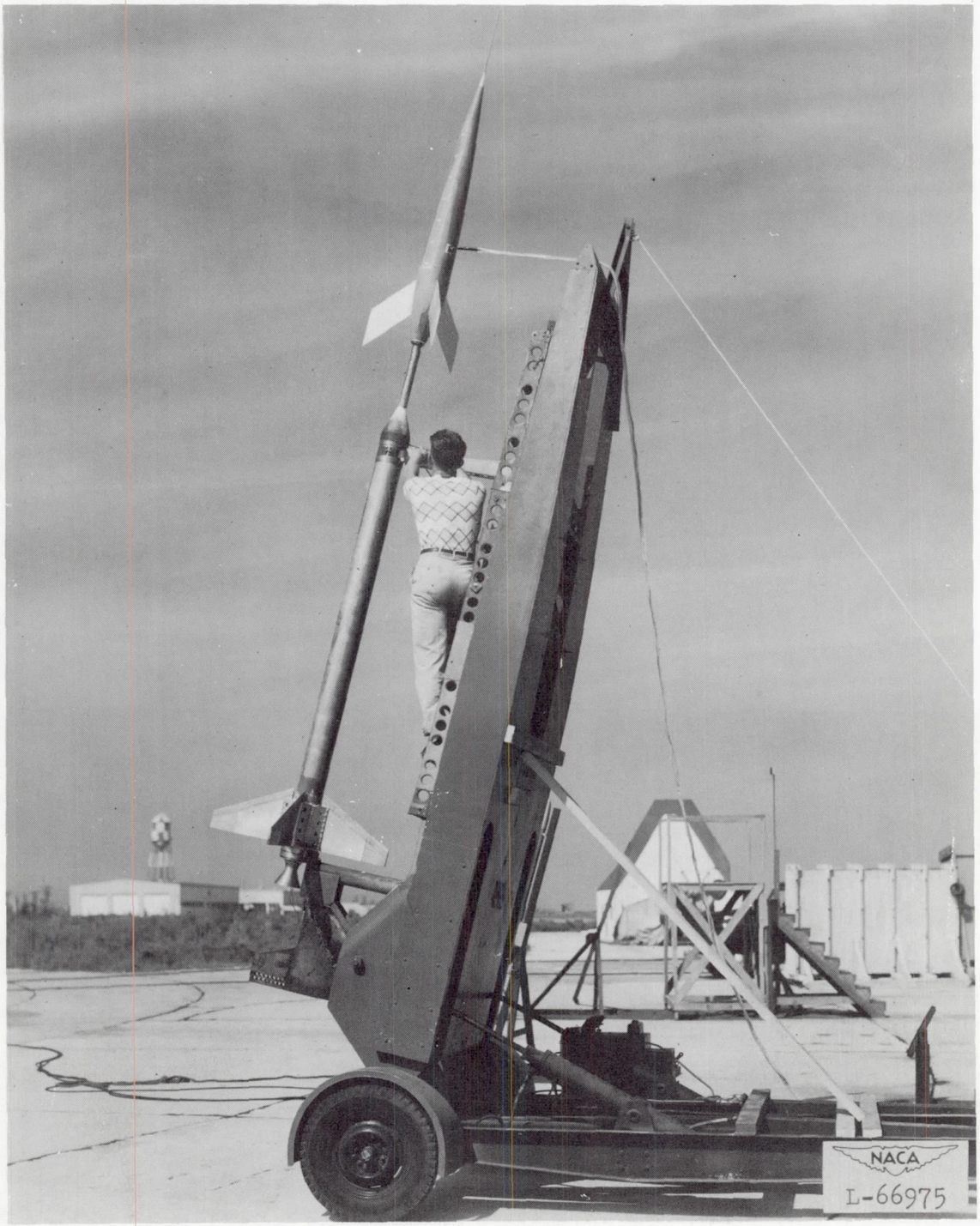

(a) Model and booster on zero length launcher.

Figure 2.- Photographs of model and booster.

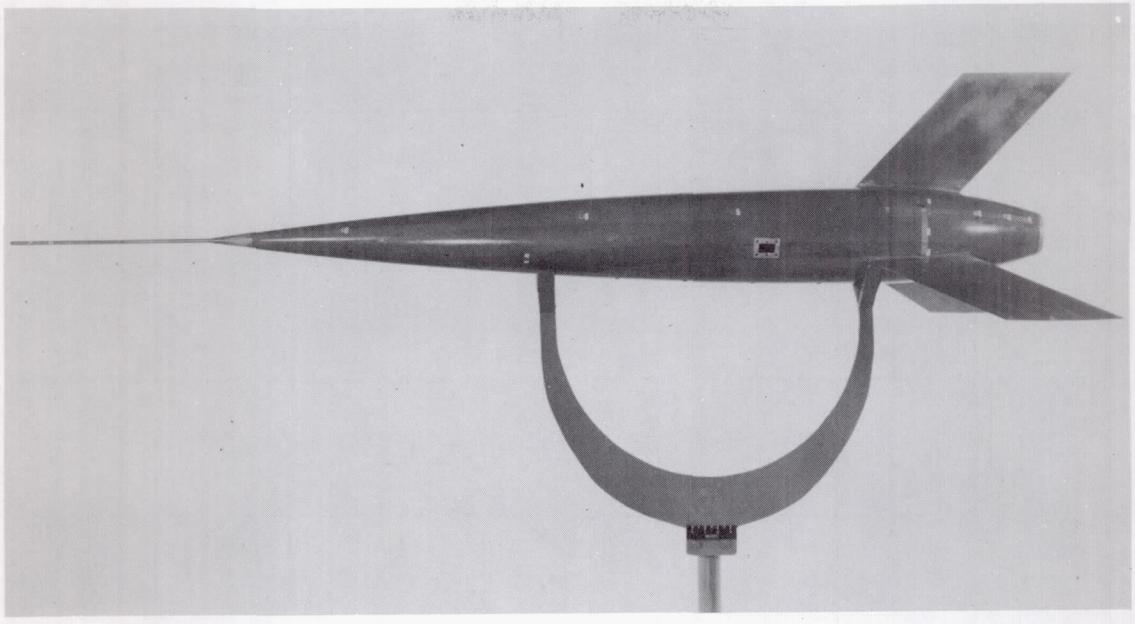

(b) Model showing position of pressure orifices. L-66953.1

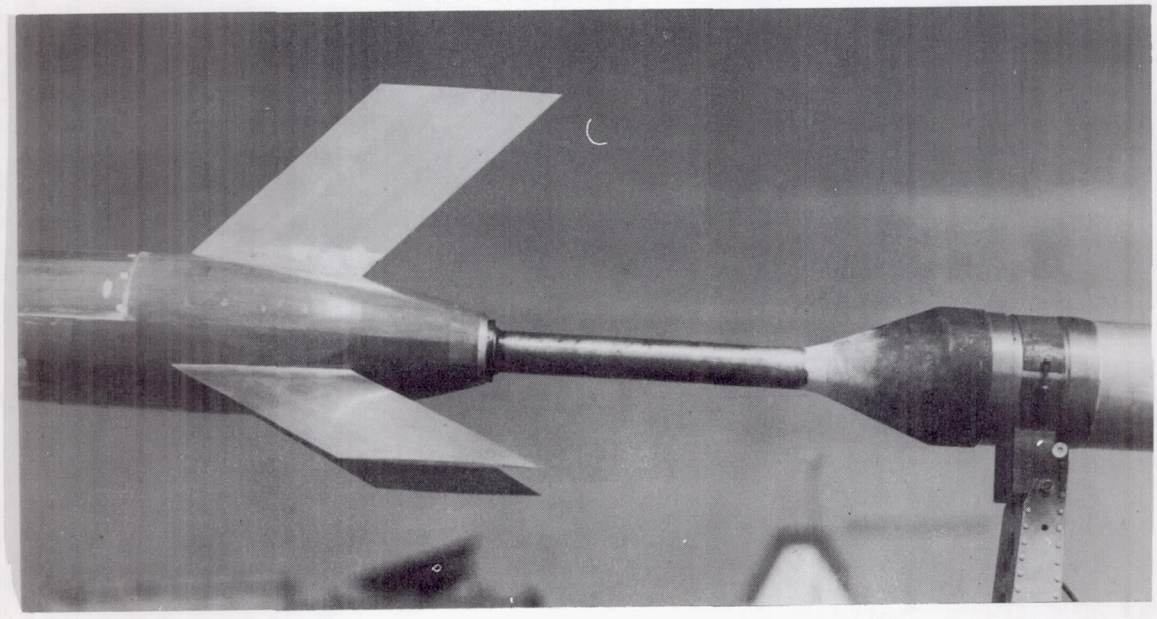

(c) Model and simulated wind-tunnel sting. L-66973

Figure 2.- Concluded.

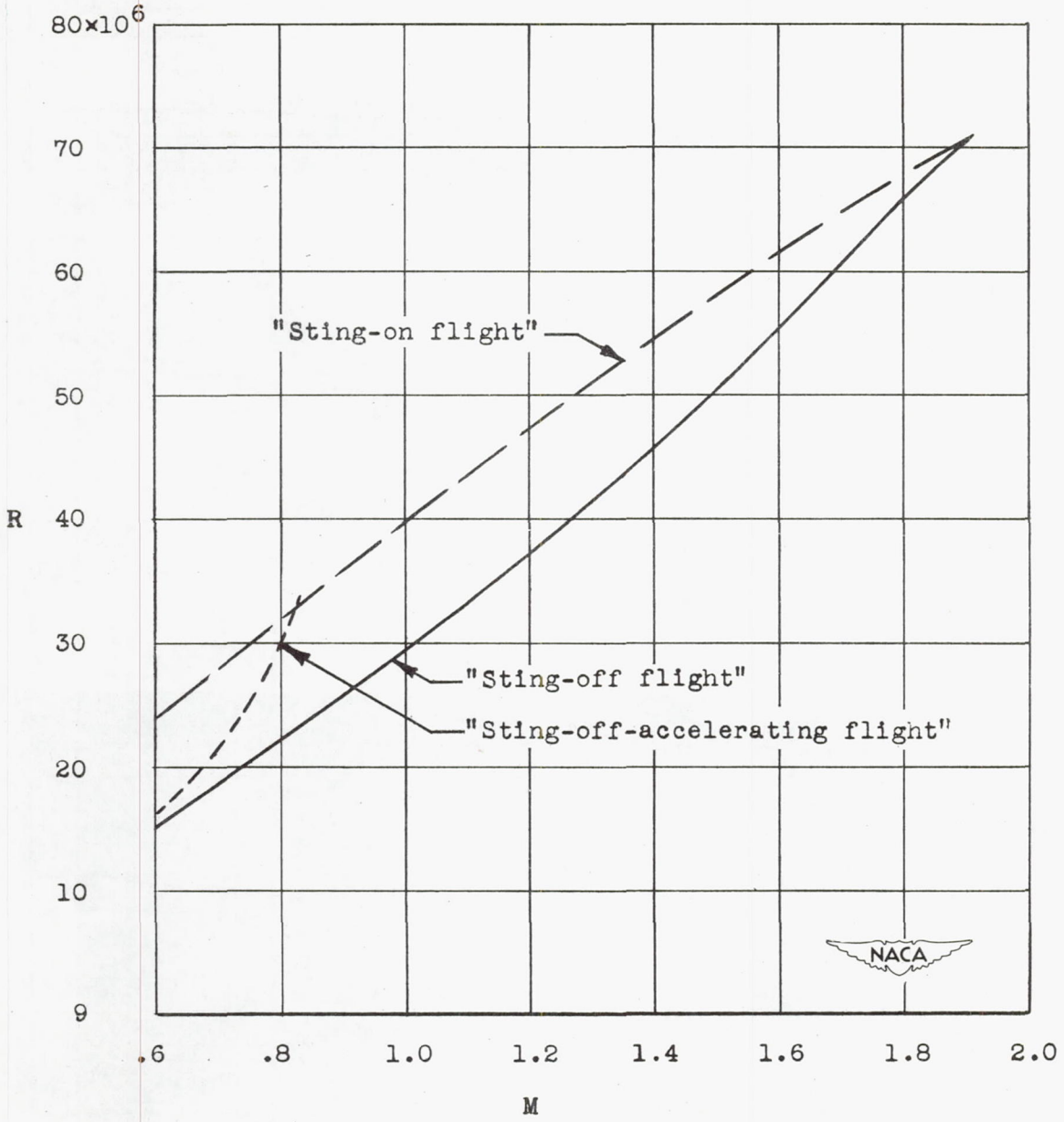

Figure 3.- Reynolds number based on body length against Mach number.

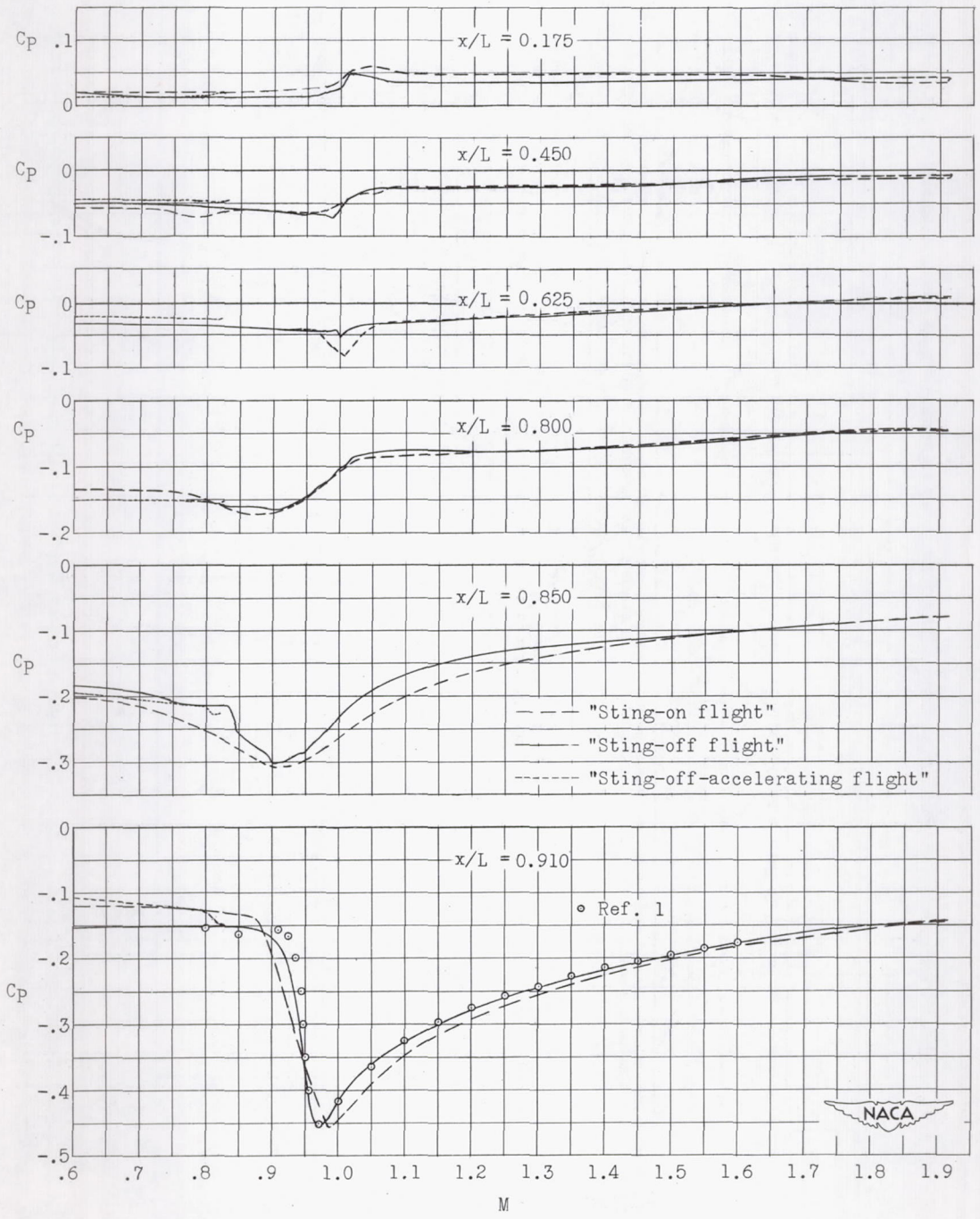

Figure 4.- Variation of pressure coefficients with Mach number. Data are presented for flight with and without the sting.

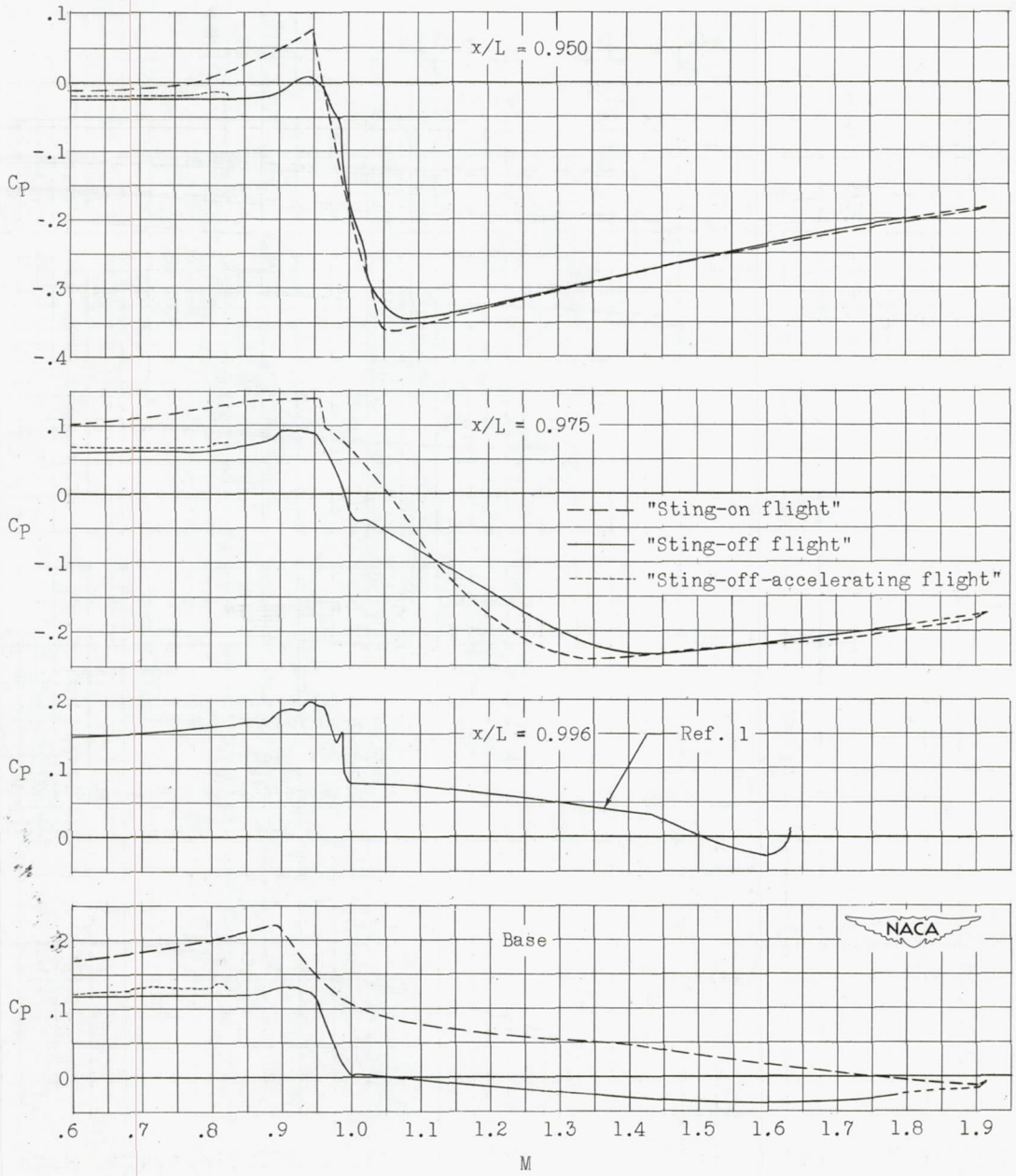

Figure 4.- Concluded.

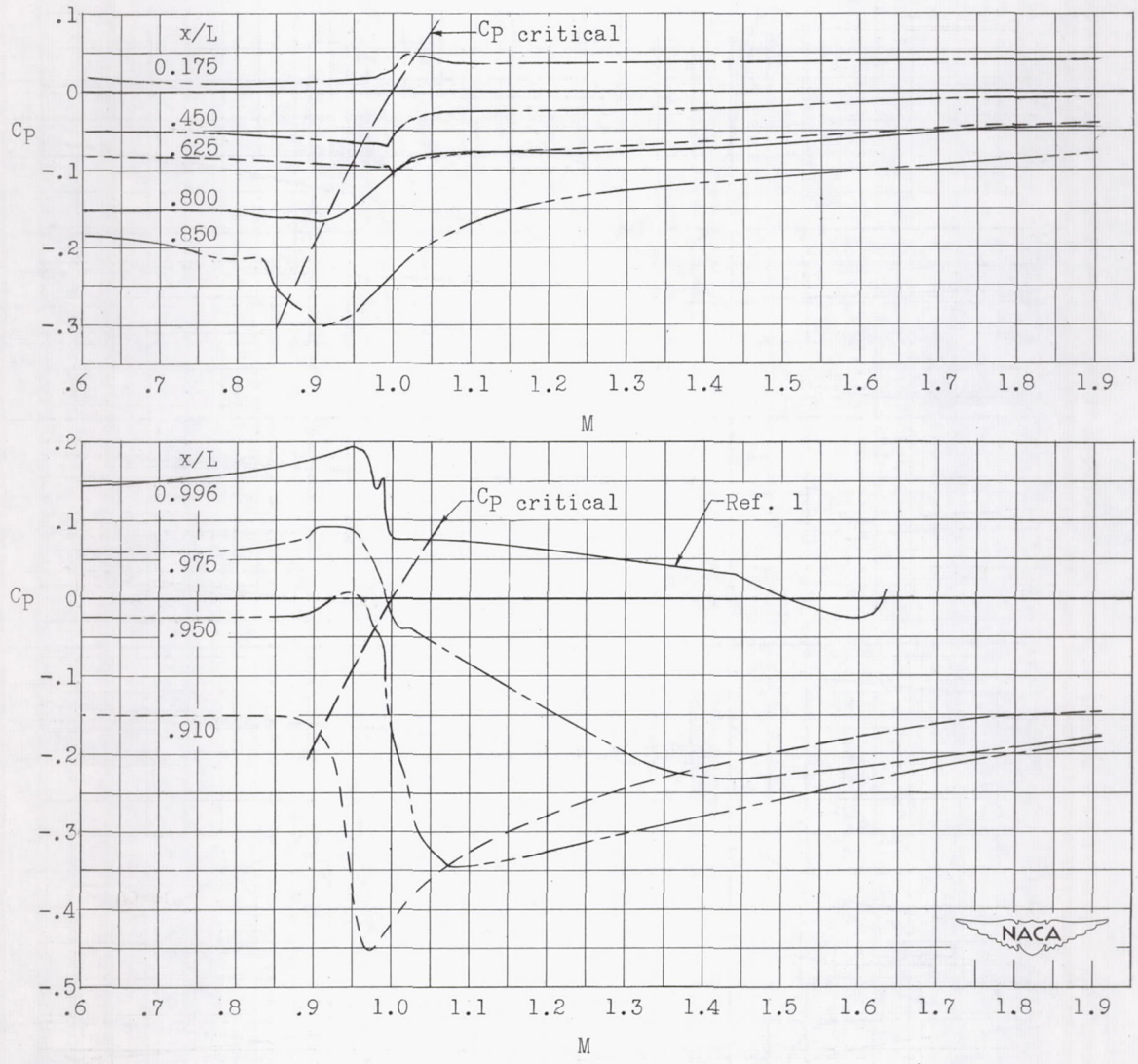

Figure 5.- Variation of "sting-off" pressure coefficient with Mach number.

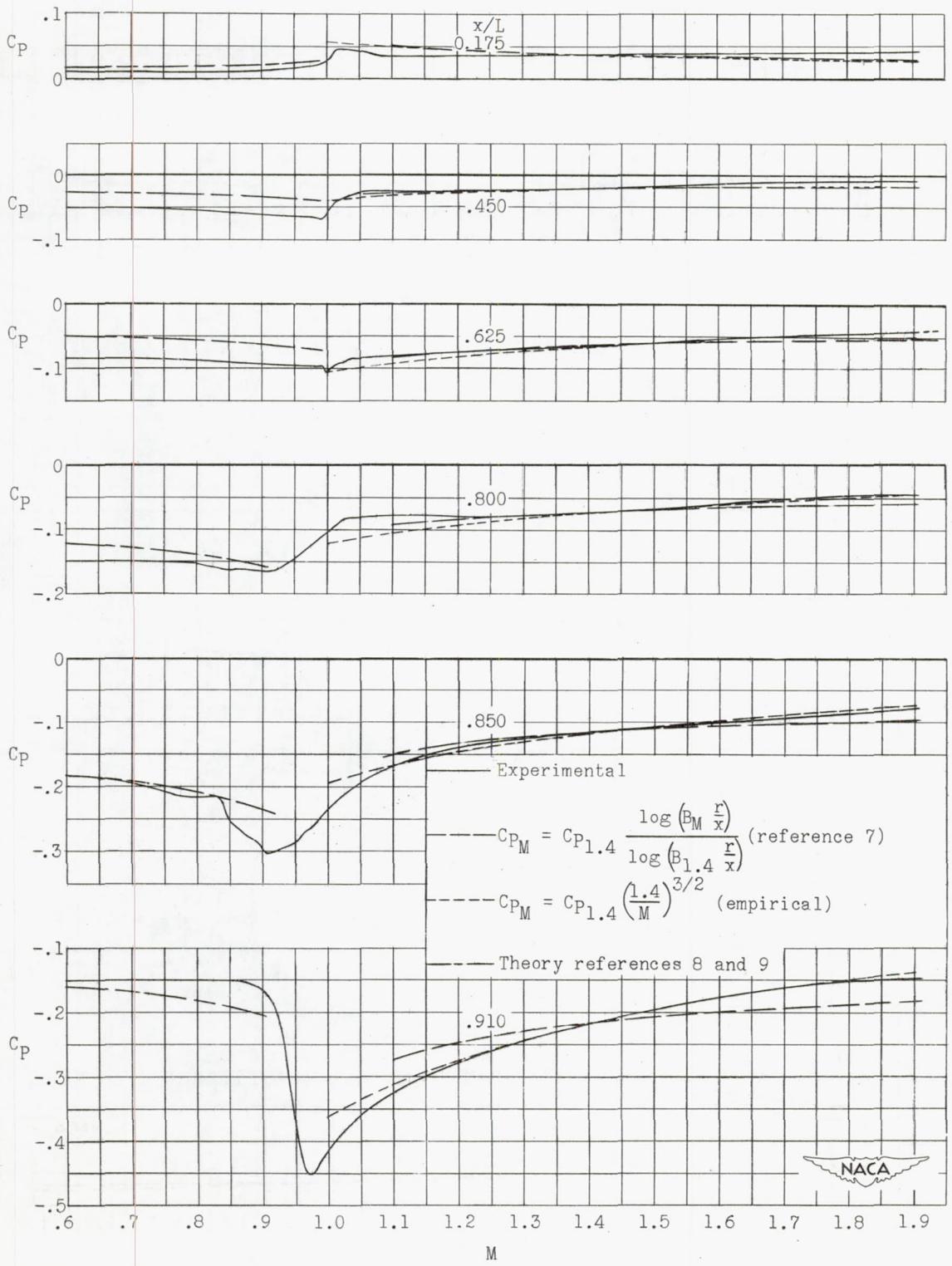

Figure 6.- The variation of "sting-off flight" pressure coefficients with Mach number compared with theoretical variations.

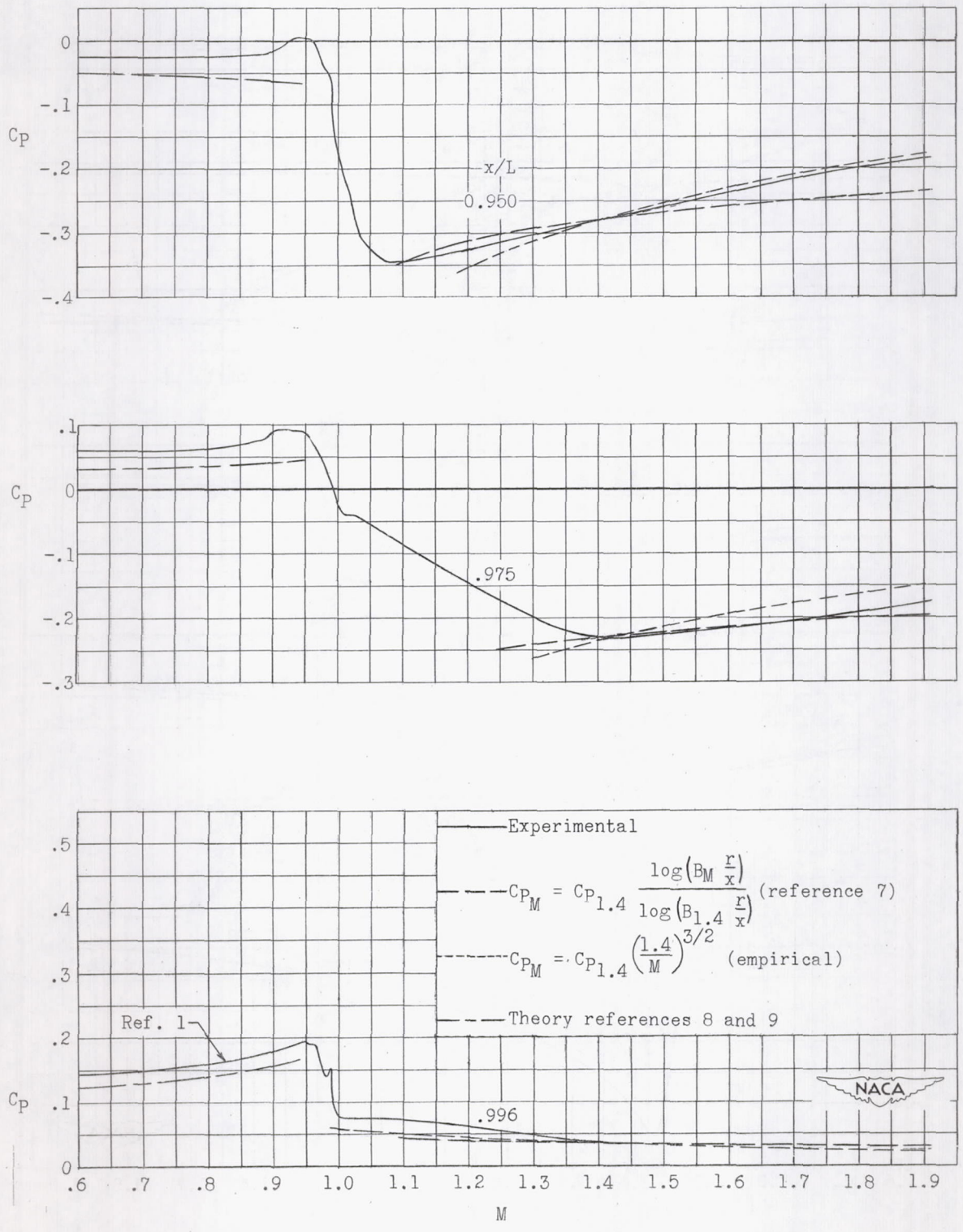

Figure 6.- Concluded.

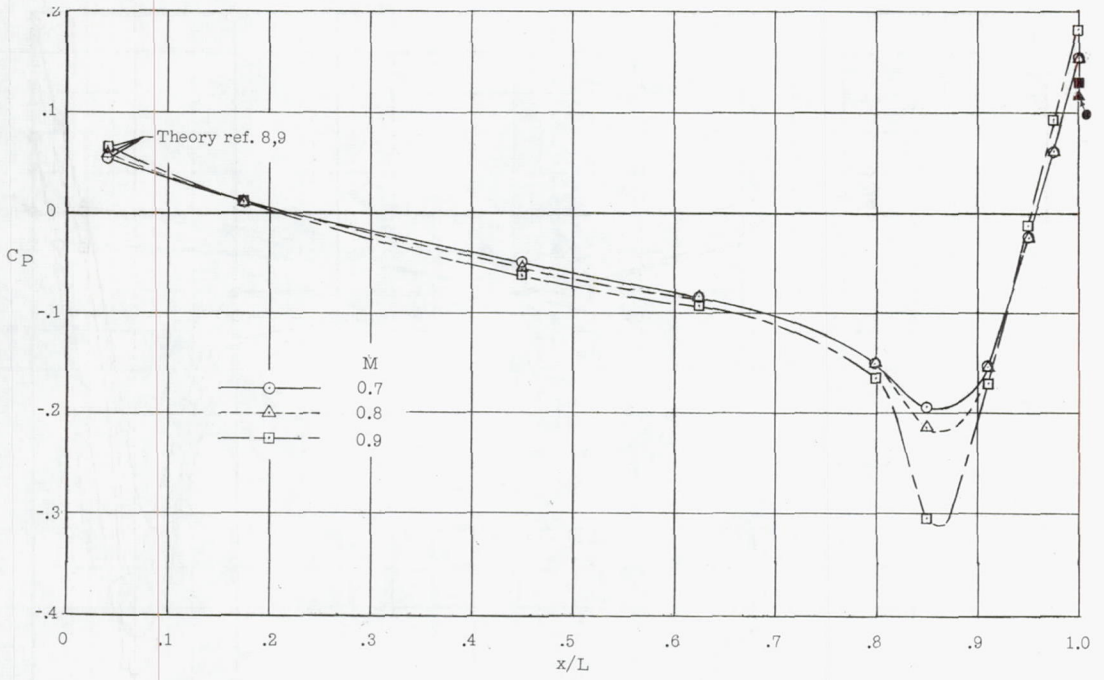

(a) Subsonic Mach numbers.

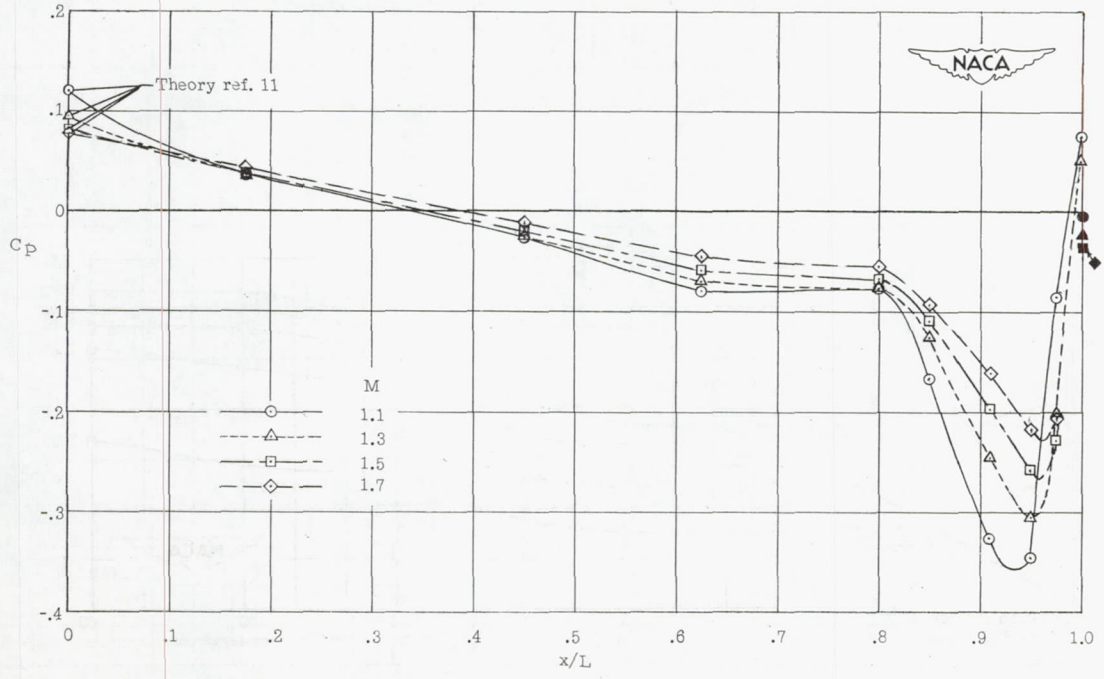

(b) Supersonic Mach numbers.

Figure 7.- Longitudinal pressure distributions against Mach number. Solid symbols show base pressure coefficients.

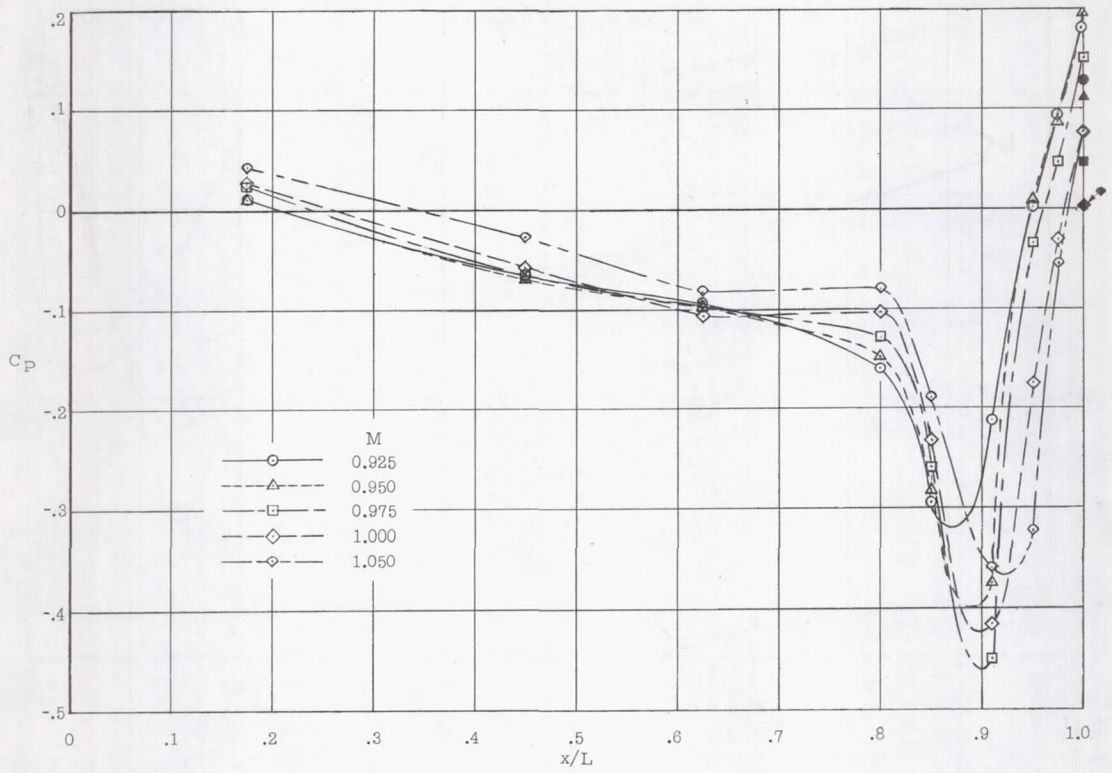

(c) Transonic Mach numbers.

Figure 7.- Concluded.

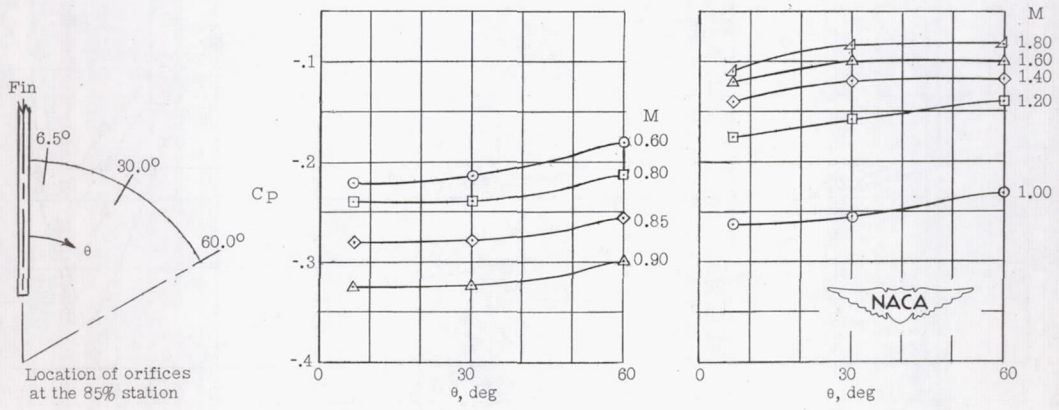

Figure 8.- Circumferential variation of the pressure coefficients at the 85-percent station.

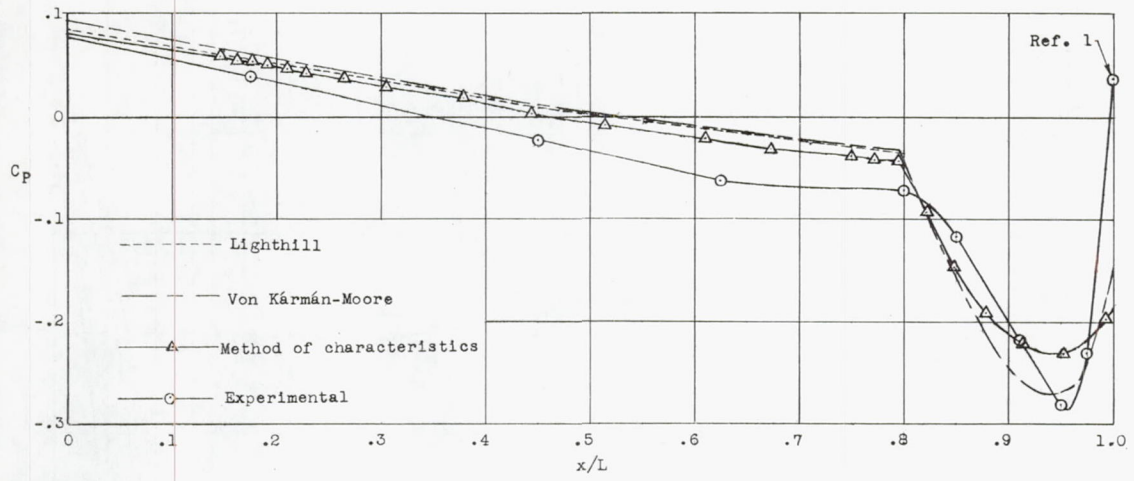

a.- M = 1.4.

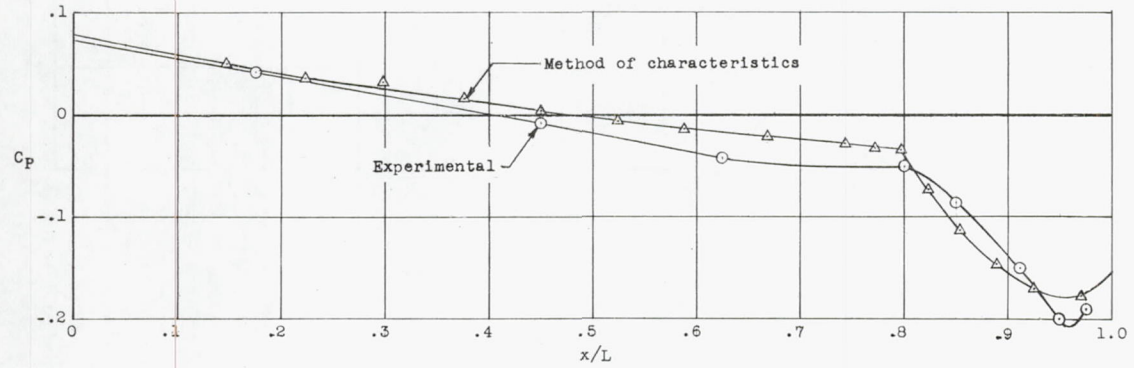

b.- M = 1.8.

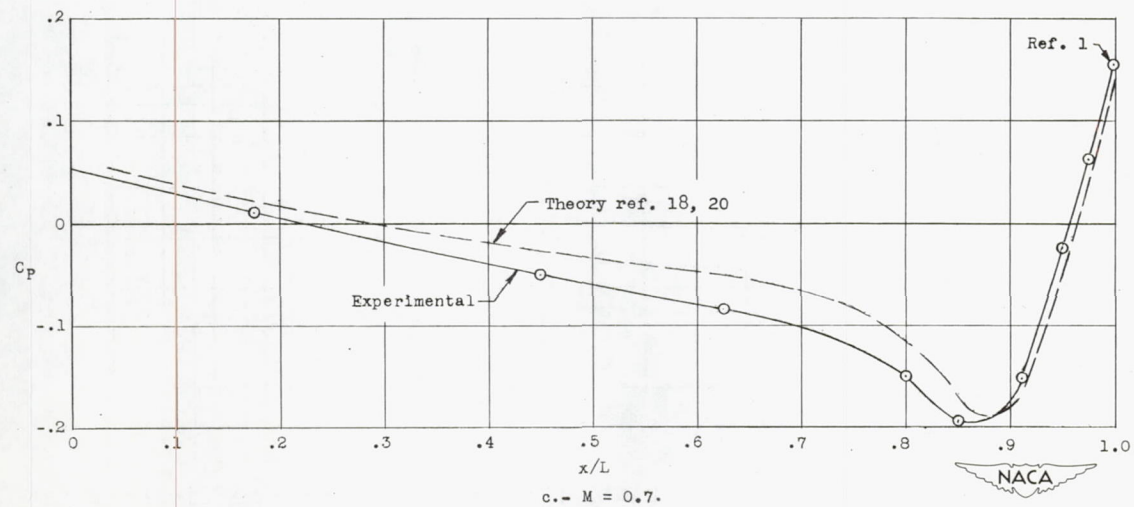

c.- M = 0.7.

Figure 9.- Experimental and theoretical pressure distributions at various Mach numbers.

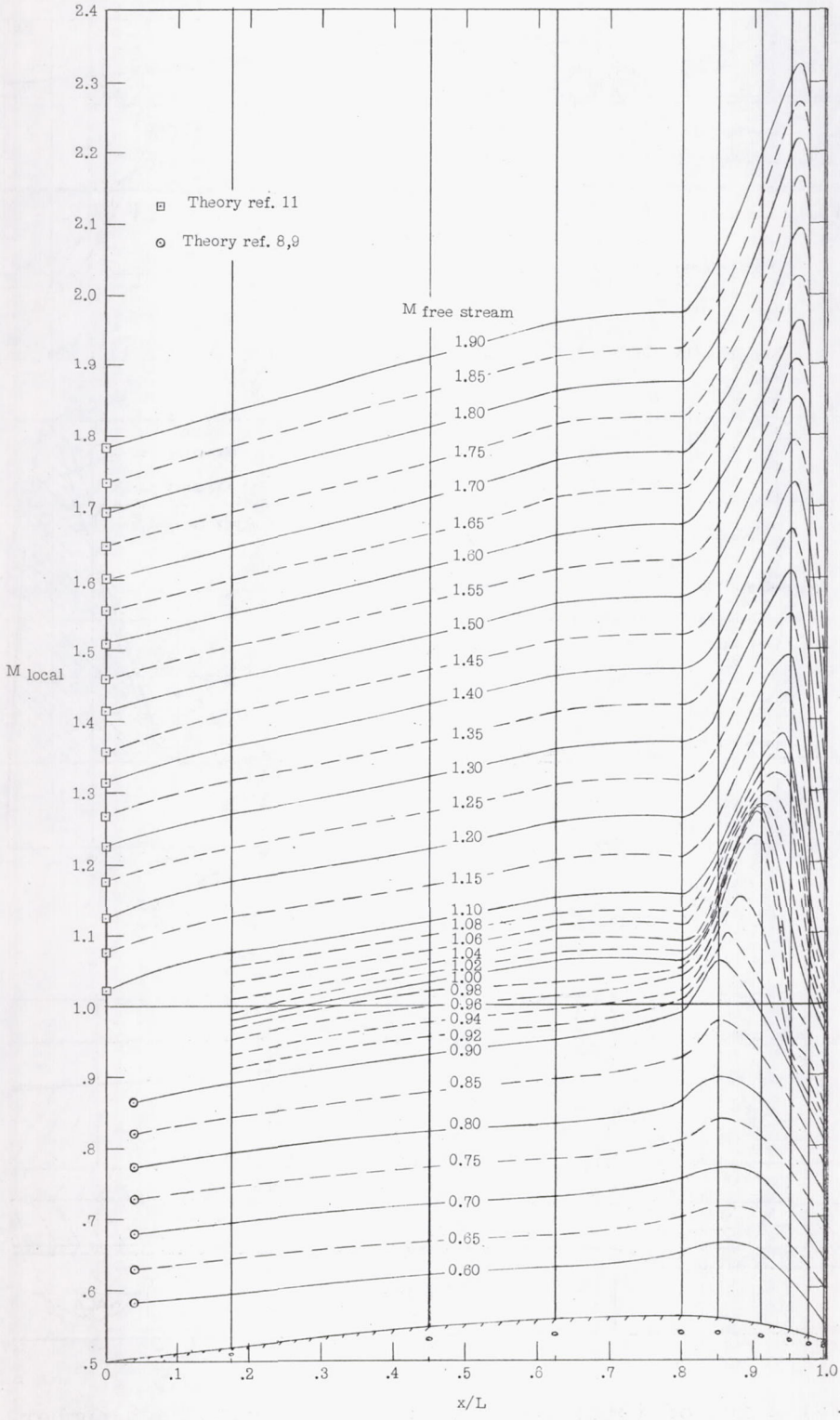

Figure 10.- Longitudinal distribution of local Mach numbers at various free-stream Mach numbers.

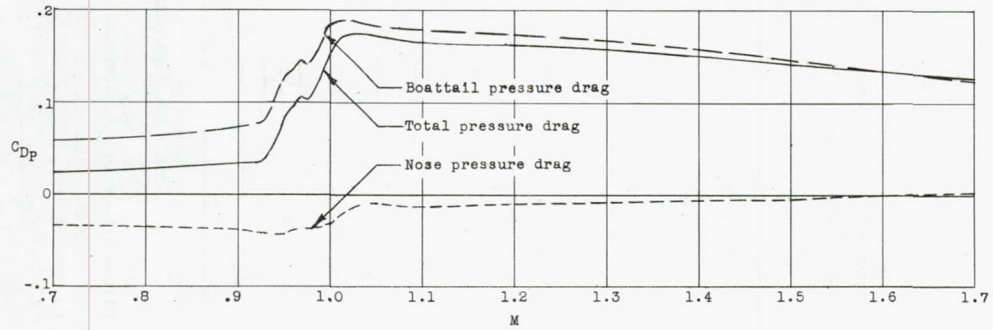

(a) Variation of nose, boattail, and total pressure drag with Mach numbers.

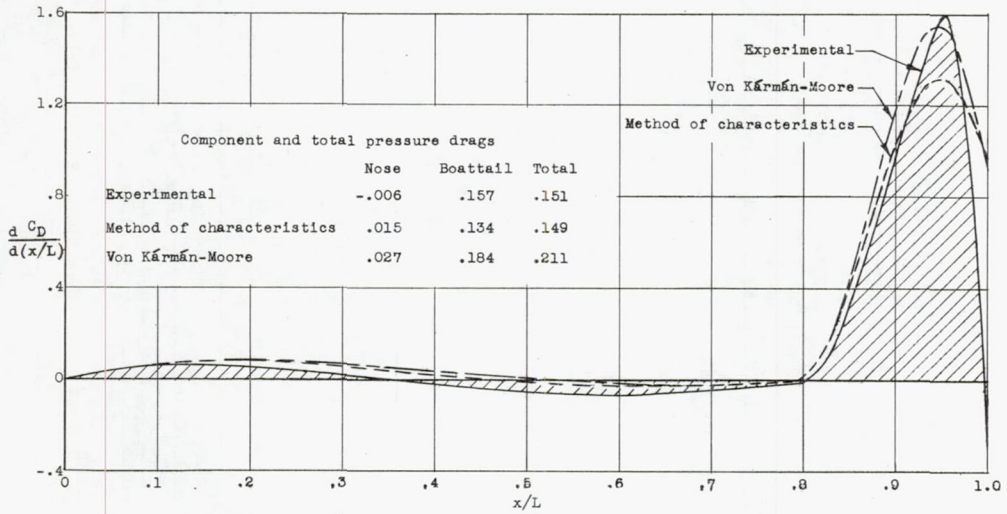

(b) Pressure-drag distribution at M = 1.4.

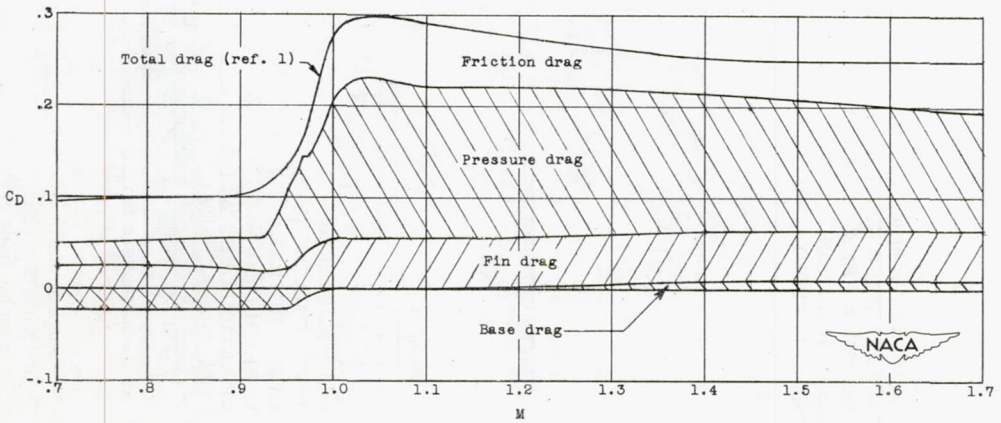

(c) Variation of total and component drags with Mach number.

Figure 11.- Variation of drag components with Mach numbers.